

## Thermal camouflages based on 3D thermal-null medium

Hanchuan Chen<sup>1</sup>, Fei Sun<sup>\*1</sup>, Bo Wang, Yichao Liu, Zihui Chen, Yibiao Yang

*Key Lab of Advanced Transducers and Intelligent Control System, Ministry of Education and Shanxi Province, College of Physics and Optoelectronics, Taiyuan University of Technology, Taiyuan, 030024, China*



### ABSTRACT

Thermal camouflage devices, which can transfer the temperature field produced by the heat target on the object plane to pre-designed illusory temperature field on the image plane, are designed by a block building approach. The building blocks are four basic thermal components, which are designed based on the 3D thermal-null medium and can individually achieve the effects of thermal shifting, splitting, compression, and deforming. 3D thermal-null medium, which performs as a good ‘thermal fiber’ and can achieve directional heat conduction along its main axis, is designed and fabricated by placing specifically oriented copper-air arrays in polyurethane plates. The proposed method provides a simple way to design thermal camouflage devices, which can simultaneously camouflage the position, quantity, size and shape of the heat target by choosing/combining different basic thermal components. All designed thermal camouflage devices of different functions can be realized by different oriented copper-air arrays in polyurethane plates. Both numerical simulations and experimental measurements verify the performance of the designed thermal camouflage devices, which may have applications on thermal image processing and thermal illusion.

### 1. Introduction

In nature, an important skill of animals is to avoid predators through various camouflage, such as color changeable properties [1], dynamic body patterns [2], and adaptive optical/sonic transparency [3]. Inspired by biological camouflages, humans have invented many camouflage techniques, such as optical Janus effect [4], bionic adaptive robots [5], and radar deception technology [6–9]. Thermal camouflage device (TCD) can camouflage the real thermal characteristics of the heat target, such as size, shape, position, and quantity, for the IR camera [10–20]. In recent years, many TCDs of various novel thermal control functions, such as thermal cloaks [21–23], thermal diodes [24], thermal coding [25], thermal encryption printing [26], thermal memory [27], thermal inversion [28], uniform heater [29], and thermal concentration [30], have been designed by transformation thermotics (TT) [31–33], which is a powerful designing method developed from transformation optics [34–40]. However, most current TCDs can only produce various in-plane thermal illusions (i.e., manipulating heat flow and temperature field distribution within 2D flat surfaces), which cannot be used directly to create out-of-plane thermal camouflages (i.e., transforming the temperature field distribution from one surface to another surface in accordance with a pre-designed distribution). In addition, the required material parameters of TCDs designed by TT are different for achieving different thermal camouflages and usually inhomogeneous anisotropic,

which need to be derived from a lot of mathematical calculations. Therefore, there is still a lack of study to design TCD that can achieve various out-of-plane thermal camouflages with simple/realizable material parameters by a simpler design process.

Based on the directional heat transfer properties of thermal-null medium (TNM) [41,42], which is derived from TT by an extreme spatial stretching transformation, a graphical design method can be used to design in-plane thermal devices [41]. The TNM is a highly anisotropic medium whose thermal conductivity is extremely large along its main axis and close to zero in other directions, which performs as an ideal ‘thermal fiber’ that can perfectly project the temperature field distribution along its main axis. In previous studies, 2D TNM has been realized (e.g., layered copper and expanded polystyrene [41,42] or copper/aluminum-air multi-layer structure [44,45]) to achieve in-plane thermal controls, such as thermal buffering [42] and thermal concentration [44]. However, there is still little research on 3D TNM and its implementation method. In this study, the 3D TNM is designed and realized by placing arrays of specifically oriented copper rods and air in polyurethane plates, whose main axis consists with the orientation of the copper rods. Based on the directional thermal projecting feature of the designed 3D TNM, some basic thermal components are designed first, which can separately realize thermal shifting, thermal splitting, thermal compression and thermal deforming. Furthermore, a series of TCDs, which can achieve various pre-designed out-of-plane thermal

*Abbreviations:* TT, transformation thermotics; TNM, thermal-null medium; TCD, Thermal camouflage device; PCT, positive temperature coefficient.

\* Corresponding author.

E-mail address: [sunfei@tyut.edu.cn](mailto:sunfei@tyut.edu.cn) (F. Sun).

<sup>1</sup> Hanchuan Chen and Fei Sun contributed equally to this work.

<https://doi.org/10.1016/j.ijthermalsci.2022.107506>

Received 13 October 2021; Received in revised form 15 January 2022; Accepted 30 January 2022

Available online 5 February 2022

1290-0729/© 2022 Elsevier Masson SAS. All rights reserved.

camouflages, are designed by combining/assembling the proposed basic thermal components.

As shown in Fig. 1a, the IR camera can observe the real thermal characteristics (i.e., temperature field distribution) of the heat target (the red sun) behind the ordinary cubic wall without using TCD. If the ordinary cubic wall is replaced by the designed TCD (Fig. 1b), which can camouflage the size, shape, position and quantity of the heat target by selecting combinations of basic thermal components with different functions, the IR camera cannot observe the real thermal characteristics of the heat target and can only obtain the pre-designed camouflaged thermal images. Unlike previous TCDs that can only produce in-plane thermal camouflages, the object plane and the image plane of the designed TCD are not in the same plane (i.e., out-of-plane thermal camouflages).

Compared with TT, the design method proposed in this study is a block building method, which only needs to select and combine basic thermal components of different functions without any coordinate transformations and tensor calculations. In addition, all out-plane TCDs with different functions can be realized by using a same material, i.e., the designed 3D TNM, which can be realized by placing copper rod-air arrays with different orientation angles and filling factors in polyurethane plates.

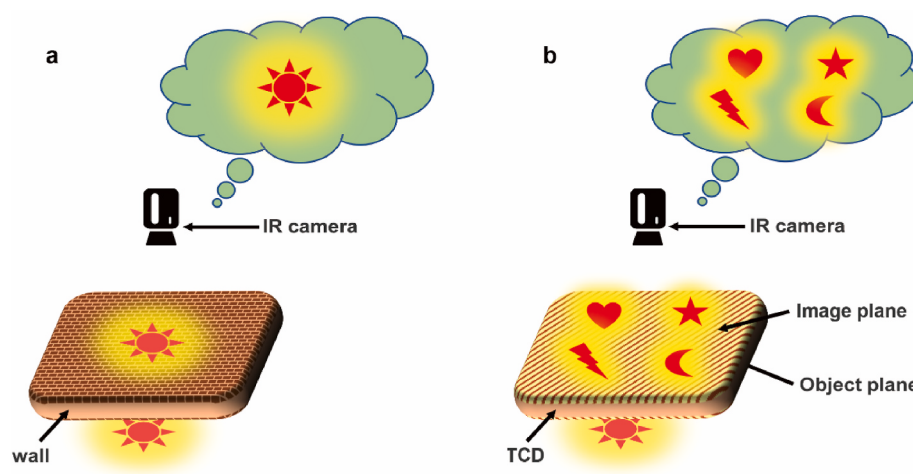
## 2. Methods and results

### 2.1. 3D TNM by copper-air arrays in polyurethane plates

Based on directional thermal conducting capability of TNM, a series of thermal devices, such as thermal cloaks, thermal rotators, and thermal concentrators, can be designed by a graphical way, i.e., designing the shapes of the object/image surfaces and the orientation of the TNM's main axis filled between them [41]. The ideal TNM, whose thermal conductivity tends to infinity along its main axis and zero in other directions, can produce perfect directional projection of heat flows and perform as a perfect 'thermal fiber' [41–44]. For example, the thermal conductivity of an ideal TNM whose main axis is along the  $x$  direction can be expressed as [41–44]:

$$k = k_0 \text{diag} \left( \frac{1}{\Delta}, \Delta, \Delta \right) \quad (1)$$

where  $\Delta \rightarrow 0$ ,  $k_0$  is a constant (e.g., the thermal conductivity of background), and  $\text{diag}$  represents a diagonal matrix. Although the ideal TNM is almost impossible to realize, there are many studies showing that the simplified TNM with large thermal conductivity along the main axis and small thermal conductivities in the other directions can still generate a good directional heat guidance effect (e.g.,  $0 < \Delta < 1$  in equation (1))



[41–44]. For example, the simplified 2D TNM can be approximately realized by layered copper and expanded polystyrene in thermal epoxy background [41,42], which has been successfully used to design 2D in-plane thermal devices. In the present work, simplified 3D TNM is designed by placing specifically oriented copper-air arrays in polyurethane plates (see Fig. 2a) based on the effective medium theory [46, 47], whose main axis consists with the orientation of the copper rods (more analytical calculations can be found in Supplementary Material Note 1). The designed 3D TNM performs as a reduced 'thermal fiber' (see Fig. 2b), which can project the temperature field from the input surface  $S_1$  in Fig. 2c to the output surface  $S_2$  in Fig. 2d along its main axis. Note that the 3D TNM's main axis (the orientations of copper rods in Fig. 2a) can be designed to change with spatial position, which in turn leads to novel thermal devices of special functions shown later.

In order to achieve the out-of-plane thermal camouflages in Fig. 1b, four types of basic thermal components with different functions are designed based on 3D TNM first. Later we will show how to combine these basic thermal components by a block building approach to achieve TCDs with various composite out-of-plane thermal camouflage functions.

### 2.2. Basic thermal components

**Thermal Shifter.** The function of thermal shifter is to camouflage the position characteristics of heat target by the 3D TNM with a fixed main axis (see Fig. 3a and b). The geometrical size of thermal shifter (i.e., length  $a$ , width  $b$  and height  $h$ ) can be designed according to the actual size of the heat target and the camouflaged distance  $d$  (i.e., the shift between the position of the heat target on the object plane and the position of the camouflaged thermal image on the image plane along the  $x$  and/or  $y$  directions).

According to the directional guiding property of 3D TNM for heat flow, the temperature field distribution on the object plane is projected along the main axis of the 3D TNM (see Fig. 3b) onto the image plane, and then a camouflaged temperature field distribution is created on the image plane where the position of the camouflaged thermal image is shifted by a pre-designed camouflaged distance  $d$ . The camouflaged distance  $d$  can be designed by choosing suitable height of the thermal shifter  $h$  and 3D TNM's main axis angle  $\theta$  (also the angle between copper rods and  $z$ -axis):

$$d = h \cdot \tan \theta \quad (2)$$

As a specific example, a thermal shifter ( $a = 0.2$  m,  $b = 0.2$  m,  $h = 0.1$  m) with camouflaged distance  $d = 7.5$  cm is designed by placing copper rods with fixed orientation in polyurethane plates (the orientation angle to  $z$ -axis is fixed at  $\theta = 37^\circ$ ), whose performance is verified by numerical

**Fig. 1.** Out of plane observation contrast diagram without or with TCD. (a) Schematic diagram of observing the heat target behind the wall by IR camera without the TCD. When the sun-shaped heat target behind the ordinary wall without the TCD, the real thermal characteristics of the heat target can be observed through the IR camera without distortion (i.e., no thermal camouflage effect). (b) Schematic diagram of observing the heat target behind the TCD by IR camera. When the sun-shaped heat target is behind the TCD, the faked thermal characteristics (e.g., position, quantity, size, and shape) of the heat target will be created on the image plane of the TCD, and then the camouflaged thermal image is observed through the IR camera.

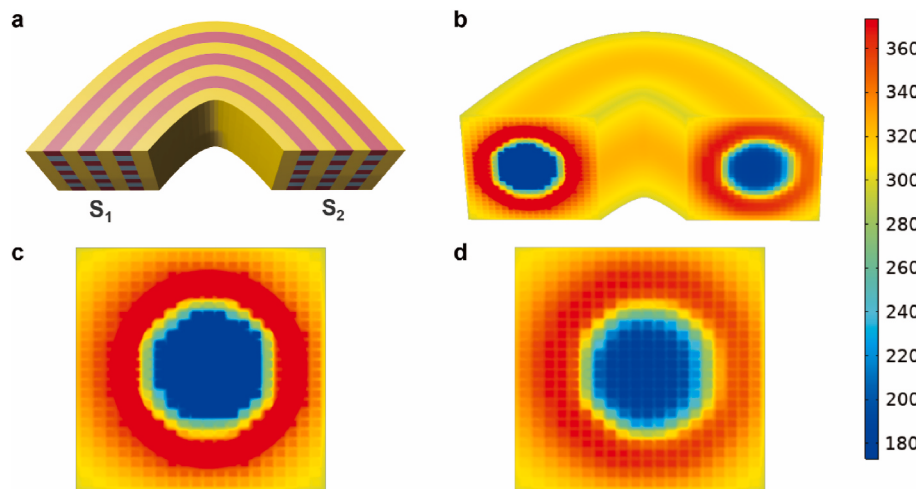


**Fig. 2.** Schematic diagram and simulated temperature field distributions of 3D TNM. (a) Schematic diagram of 3D TNM by placing specifically oriented copper-air arrays in polyurethane plates. The copper rods (colored red) and air (colored gray) with volume ratio 1:1 form a basic unit broad, which is then staggered with polyurethane boards (colored yellow) with a filling factor 1:1 to perform as simplified 3D TNM. (b)–(d) the simulated temperature field distributions inside the whole 3D TNM (b), at the input surface  $S_1$  (c), and at the output surface  $S_2$  (d) when an annular heat source is distributed on the input surface of the designed 3D TNM. Other numerical settings can be found in Supplementary Material Note 2. (For interpretation of the references to color in this figure legend, the reader is referred to the Web version of this article.)

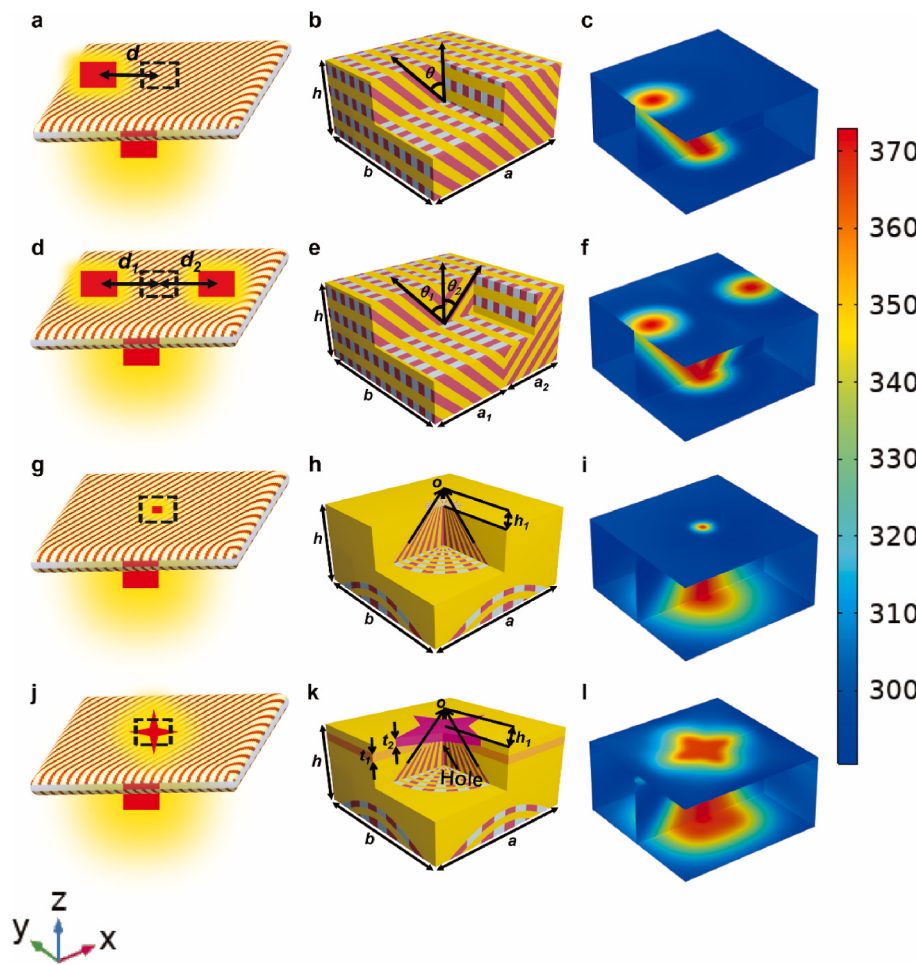


**Fig. 3.** The schematic diagram, structural schematics and temperature field distributions by numerical simulations for four basic thermal components. The schematic diagram of out-of-plane thermal camouflages for four basic thermal components: (a) thermal shifter, (d) thermal splitter, (g) thermal compressor, and (j) thermal deformer. To clearly contrast the camouflaged thermal image on the image plane with the original heat target on the object plane, the black dashed square on the image plane is introduced to indicate relative position and size of the heat target. The structural schematics of the basic thermal components by placing specifically oriented copper rods (colored red) and air (colored gray) to form a basic unit broad and then being staggered with polyurethane boards (colored yellow): (b) thermal shifter, (e) thermal splitter, (h) thermal compressor, and (k) thermal deformer. The temperature field distributions by numerical simulations for four basic thermal components: (c) thermal shifter, (f) thermal splitter, (i) thermal compressor, and (l) thermal deformer. Details on numerical settings can be found in Supplementary Material Note 2. (For interpretation of the references to color in this figure legend, the reader is referred to the Web version of this article.)

simulation in Fig. 3c. As shown in Fig. 3c, the camouflaged temperature field distribution on the image plane is the same as translating the temperature field distribution on the object plane by the pre-designed camouflaged distance  $d = 7.5$  cm along the  $x$  direction, which verifies the expected thermal shifting effect. The thermal shifter can produce a camouflaged thermal image with the same thermal characteristics of the real heat target except that the spatial location is different from the real heat target.

**Thermal Splitter.** The function of thermal splitter is to camouflage quantity characteristics of heat target by the designed 3D TNM. As shown in Fig. 3d, thermal splitter can split the heat flow generated by a single heat target on the object plane into two parts, and consequently creating two new camouflaged thermal images on the image plane. The thermal splitter can be designed by using two thermal shifters with opposite shifting directions (i.e., copper rods with different orientations  $\theta_1$  and  $\theta_2$  in Fig. 3e). The geometrical size of thermal splitter (i.e., length

$a = a_1 + a_2$ , width  $b$  and height  $h$ ) can be designed according to the actual size of the heat target and the separation distance  $D$ , which is the distance between two new camouflaged thermal images on the image plane.

If a heat target is located at the center on the object plane of the thermal splitter, the temperature field distribution on the object plane will be guided by two 3D TNMs along the two divergent directions onto the image plane, and then a camouflaged temperature field distribution is formed on the image plane where two new camouflaged thermal images are created with a pre-designed separation distance  $D$ . The separation distance  $D$  can be designed by choosing suitable height of the thermal shifter  $h$  and the angles between copper rods and  $z$ -axis of two thermal shifters ( $\theta_1$  and  $\theta_2$  in Fig. 3e):

$$\begin{cases} D = d_1 + d_2 \\ d_1 = h \cdot \tan \theta_1 \\ d_2 = h \cdot \tan \theta_2 \end{cases} \quad (3)$$

As a specific example, a thermal splitter ( $a_1 = a_2 = 0.1$  m,  $b = 0.2$  m,  $h = 0.1$  m) with separation distance  $D = 15$  cm is designed by placing copper rods with fixed orientation angles  $\theta_1 = \theta_2 = 37^\circ$  in polyurethane plates, whose performance is verified by numerical simulation in Fig. 3f. As shown in Fig. 3f, the real heat target on the object plane is split into two parts by the pre-designed distance  $d_1 = d_2 = 7.5$  cm along the  $x$  direction, and creates two new camouflaged thermal images with separation distance  $D = 15$  cm on the image plane. Note that the positions of two new camouflaged thermal images can be separately designed and do not need to be symmetrical (i.e.,  $\theta_1 = \theta_2$  is not a necessary condition).

**Thermal Compressor.** The function of thermal compressor is to camouflage the size characteristics of heat target. As shown in Fig. 3g, thermal compressor can compress the temperature field distribution by the heat target on the object plane, and create a camouflaged temperature field distribution on the image plane that is the same as the temperature field produced by a camouflaged thermal image whose size are smaller than the heat target. The geometrical size of thermal compressor (i.e., length  $a$ , width  $b$ , and height  $h$ ) can be designed according to the scaling ratio  $M = h_1/(h_1 + h)$ , which also determines the ratio of the camouflaged thermal image's size to the heat target's size.

As a specific example, a thermal compressor ( $a = 0.2$  m,  $b = 0.2$  m,  $h = 0.1$  m,  $h_1 = 0.02$  m) is designed by using copper rods with gradual orientations in polyurethane plates, whose orientation angles are along the radial direction in the spherical coordinate system (the origin of the spherical coordinate system  $O$  is the point  $h_1$  above the center of the image plane in Fig. 3h). The performance of the thermal compressor is verified by numerical simulation in Fig. 3i, which shows that the temperature field distribution on the image plane is a compressed map of the temperature field distribution on the object plane, and therefore the outside observers will see a camouflaged thermal image with a reduced size. The thermal compressor can produce a shrunken thermal image with the same thermal characteristics of the real heat target except that the size is the compression of the real heat target.

**Thermal Deformer.** The function of thermal deformor is to camouflage the shape characteristics of heat target (see Fig. 3j), which can be realized by adding a modification layer on top of the thermal compressor (see Fig. 3k). The 3D TNM inside the lower structure of the thermal deformor is the same as a thermal compressor with length  $a$ , width  $b$  and height  $(h - t_1 - t_2)$ , where the orientation angles of copper rods are along the radial direction in the spherical coordinate system whose origin  $O$  is  $h_1$  above the center of the image plane. The upper modification layer of the thermal deformor consists of two parts: the isolation layer and the deformation layer. The isolation layer (colored orange in Fig. 3k) is a polyurethane plate of thickness  $t_1$  with a hole in its center, whose function is to prevent the interaction between the camouflaged thermal image on the image plane and the heat target on the object plane. If the thickness of the isolation layer is too thin (e.g.,  $t_1 < 0.01h$ ), the camouflaged thermal image on the image plane will in turn affect the temperature field distribution on the object plane (see Supplementary

Material Note 3 for the selection of the isolation layer's thickness). The material in the hole of the isolation layer is 3D TNM, whose main axes are oriented as an extension of the thermal compressor below. The shape and size of the hole are consistent with the heat target on the object plane. The deformation layer (colored yellow in Fig. 3k) is a special shaped copper sheet (e.g., the rosy star in Fig. 3k) embedded in a polyurethane plate of thickness  $t_2$ , whose function is to create the camouflaged thermal image with pre-designed shape. The geometrical shape of copper sheet, which determines the shape of the camouflaged thermal image on the image plane, can be designed freely provided that the its area is bigger than the area of the hole in the isolation layer.

As a specific example, the function of a thermal deformer ( $a = 0.2$  m,  $b = 0.2$  m,  $h = 0.1$  m,  $h_1 = 0.02$  m,  $t_1 = 0.01$  m,  $t_2 = 0.01$  m, and the size of the hole in the isolation layer is  $10 \times 10 \times 10$  mm<sup>3</sup>) is verified by numerical simulation in Fig. 3l, which shows that the temperature field distribution on the image plane looks like a camouflaged thermal image whose shape is the same as the copper sheet in the deformation layer, and no longer the same as the real heat target (a square aluminum sheet).

### 2.3. TCDs by the combination of basic thermal components

TCDs, which can create various out-of-plane thermal camouflages (i.e., simultaneously camouflage the thermal characteristics like location, quantity, size, and shape of heat target as needed), can be achieved by choosing and combining above designed four basic thermal components. As an example, a TCD, which can transfer one square heat target on the object plane to two star-shaped thermal images on the image plane, is designed by combining one thermal splitter and two thermal deformers (see Fig. 4a and b). The TCD in Fig. 4b can firstly split the temperature field distribution on the object plane generated by one square heat target into two parts through one thermal splitter ( $a_1 = a_2 = b = 0.2$  m,  $h_s = 0.1$  m, and the orientation angles of copper rods to  $z$ -axis are chosen as  $\theta_1 = \theta_2 = 45^\circ$ ) in the region II, and then reshape the temperature field distribution on the middle interface by two deformers ( $t_d = 0.05$  m,  $t_1 = 0.005$  m,  $t_2 = 0.01$  m, and orientation angles of copper rods are along the radial directions in two spherical coordinate systems with origins  $O_1$  and  $O_2$ ,  $h_1 = 0.02$  m above the image plane) in the region I, and finally produce two star-shaped camouflaged thermal images with different shapes and sizes from the heat target on the image plane (see numerical result in Fig. 4c). The shape of the camouflaged thermal image can be designed freely by choosing various copper sheets in the deformation layer of the thermal deformer. Another example of TCD (all geometrical dimensions are the same as in Fig. 4a, except that the shape of the copper sheet in the deformation layer changes) is given in Fig. 4d-f, which can transfer one square heat target to two Irregular polygonal camouflaged thermal images.

Four basic thermal components with different individual functions (i.e., thermal shifter for camouflaging position, thermal splitter for camouflaging quantity, thermal compressor for camouflaging size, and thermal deformer for camouflaging shape) can be used as 'building blocks' in our design method. By a block building approach (i.e., freely choosing/combing these four basic thermal components), TCDs with different composite functions can be designed (See Supplementary Material Note 4 for some other examples of TCDs).

Note that the combinations of thermal components in different orders may influence the overall functionality of the camouflage device. If the thermal camouflage devices in Fig. 4c are designed by a reverse order (e.g., the first component is deformer, and the second component is splitter), the camouflage devices cannot keep the same overall camouflage effects with some different field distributions on the image planes (See Fig. S6 in Supplement Note 6).

In Fig. 4, the square heat sources are chosen as the heat target to check the performance of the designed TCDs. If the heat target is chosen as some other shapes (i.e., no longer the square heat source), the TCD can still create the same pre-designed thermal camouflages (See

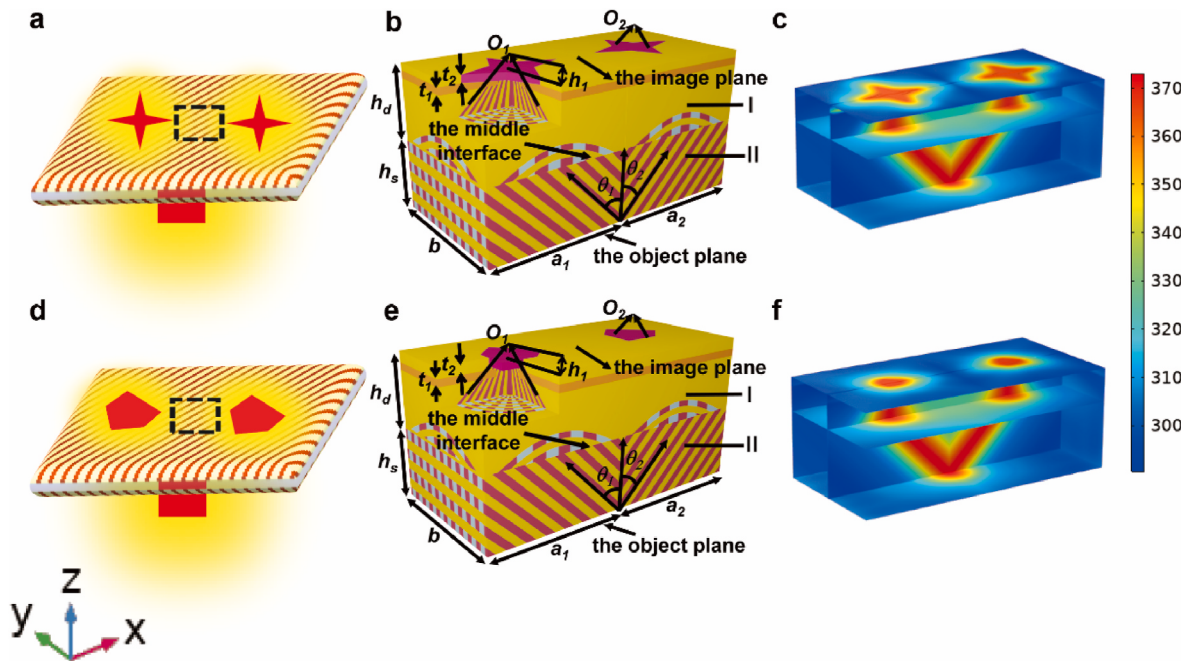


**Fig. 4.** The schematic diagram, structural schematics and temperature field distributions by numerical simulations of out-of-plane thermal camouflages by TCDs. (a) and (d) the schematic diagram of out-of-plane thermal camouflages by TCDs that can transform a square heat target on the object plane into two star-shaped images (a) and two irregular polygonal images (d), respectively. To clearly contrast the camouflaged thermal image on the image plane with the original heat target on the object plane, the black dashed square on the image plane is introduced to indicate relative position and size of the heat target. (b) and (e) the structural schematics of the TCDs to realize the pre-designed thermal camouflages in (a) and (b), respectively. The copper rods, air, polyurethane boards, and copper sheet are indicated by red, gray, yellow/orange, and rosy. (c) and (f) the temperature field distributions by numerical simulations for the TCDs in (a) and (b), respectively. The information on numerical settings can be found in Supplementary Material Note 2. (For interpretation of the references to color in this figure legend, the reader is referred to the Web version of this article.)

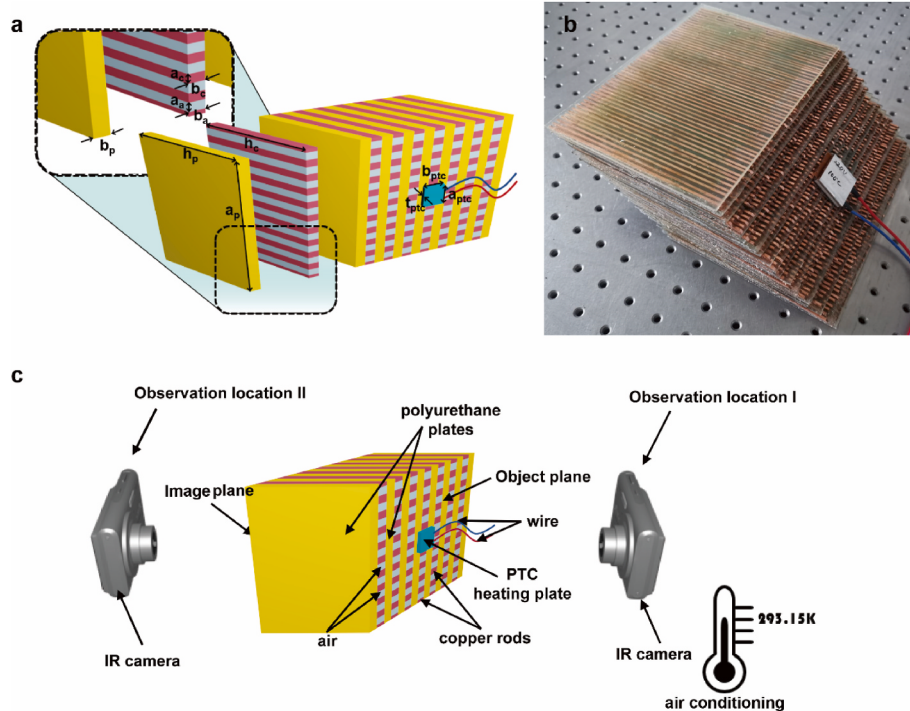


**Fig. 5.** Schematic diagram and photo of the sample and heat target and Experimental setups of the proposed scheme. (a) Schematic diagram of the sample and heat target. (b) The photo of the sample and heat target on the anti-vibration platform. (c) Schematic diagram of the experimental setup. The PTC heating plate (colored light blue) is powered by two wires (colored blue and red) connected to an external power supply. (For interpretation of the references to color in this figure legend, the reader is referred to the Web version of this article.)

Supplement Note 7), which means the performance of the designed TCD is independent of the shape of the heat target.

### 3. Experimental design and measurement results

Considering the ease of fabrication and the accuracy of processing, we make a sample of the thermal shifter manually and design an experiment to verify its out-of-plane thermal camouflage effect. The schematic diagram of the fabricated sample is shown in Fig. 5a, where copper rods with the cross-section ( $a_c = 2 \text{ mm}$ ,  $b_c = 2.82 \text{ mm}$ ) and length  $h_c = 141.4 \text{ mm}$  were arranged in arrays with air spacing ( $a_a = 2 \text{ mm}$ ,  $b_a = 2.82 \text{ mm}$ ) and then inserted into the polyurethane boards ( $a_p = 200 \text{ mm}$ ,  $b_p = 2.82 \text{ mm}$ , and  $h_p = 141.4 \text{ mm}$ ) to form a thermal shifter (see the photos in Fig. 5b). Glue was used to bond the copper rods to polyurethane boards, which was also used to fix the heat target on the object plane of the thermal shifter (more details on sample preparation can be found in Supplementary Material Note 5). The heat target is a positive temperature coefficient (PTC) heating plate ( $a_{\text{ptc}} = b_{\text{ptc}} = 30 \text{ mm}$ , and  $t_{\text{ptc}} = 6 \text{ mm}$ ), which can provide a constant temperature of 366.48 K under the condition of 220 V voltage supply.

The experimental setup is shown in Fig. 5c, where the whole experimental setup is located in an airtight room to minimize the effect of surrounding air convection, where the room temperature is kept at 293.15 K by air conditioning. The heat target (PTC heating plate) at the center of the object plane reached a stable high temperature (366.48 K) after about 22 min of power supply, and about 3–5 min later the temperature field distribution on the object plane reached thermal steady state. At this time, the temperature field distribution on the object plane was recorded by IR camera (FOTRIC 288). Then, the sample was rotated by 180° to record the temperature field distribution on the image plane (more details of the measurement process can be found in Supplementary Material Note 5 and Supplementary Movie 1).

Supplementary data related to this article can be found online at <https://doi.org/10.1016/j.ijthermalsci.2022.107506>

The measured results of the fabricated thermal shifter are shown in Fig. 6c and d, which consist well with the corresponding simulated results in Fig. 6a and b and verify the thermal shifting effect of the designed thermal shifter. To save materials and reduce fabrication time, the actual samples were not made as wide as those used in the simulations, so the presence of white areas (where the material is air) in Fig. 6c and d, which does not affect the verification of the thermal shifting

performance. The thermal characteristics produced by the heat target on the object plane can be guided by the thermal shifter in a pre-designed manner (i.e., along the main axis of the 3D TNM, which is the direction of the copper rods here), and then a shifted camouflaged thermal image is created on the image plane as designed in advance. The temperature field distribution on the image plane in Fig. 6d is like translating the temperature field distribution on the object plane in Fig. 6c by the pre-designed distance  $d = h \cdot \tan\theta = 0.1 \text{ m}$  along the  $x$  direction, which verifies the thermal shifter can camouflage the position characteristics of heat target.

Since the power wires (i.e., red and blue lines in Fig. 5b) of the PTC heating plate are copper wires with good thermal conductivity, there are two thin lines around the heat source image in Fig. 6c. Although the geometry of the PTC heating plate is square, the temperature fields on the object/image plane in both measurements and simulations diverge in an elliptical shape (see Fig. 6). This is due to the fact that the cross sections of copper rods on the object/image plane are rectangular rather than square (there is a 45° cutting angle at both ends of each copper rod during the fabrication; see Sample Preparation in Supplementary Material Note 5), which in turn makes the thermal conductivity anisotropic on the object/image plane. Some dots appear in the measured temperature field distributions in Fig. 6c and d, which is due to the different surface emissivity of copper and polyurethane ( $\epsilon_{\text{copper}} = 0.04$  and  $\epsilon_{\text{polyurethane}} = 0.945$ ) [48,49]. Similarly, since the PTC heating plate is made of aluminum, which has a low surface emissivity ( $\epsilon_{\text{aluminum}} = 0.04$ ) [48], this resulted in the measured middle temperature of the PTC heating plate in Fig. 6c not being as high as in the simulation in Fig. 6a.

### 4. Conclusion

In this study, the simplified 3D TNM is designed and implemented by placing specifically oriented copper-air arrays in polyurethane plates, which performs as a good ‘thermal fiber’ for directional heat conduction. With the help of the proposed 3D TNM, four basic thermal components including thermal shifter, splitter, compressor and deformer are designed in a graphical way, which can individually achieve out-of-plane thermal camouflage effects on location, quantity, size, and shape of the heat target. TCDs, which can simultaneously camouflage the position, quantity, size, and shape of the heat target and create pre-designed camouflaged thermal image, can be designed by combining these basic thermal components in a block building approach. Compared

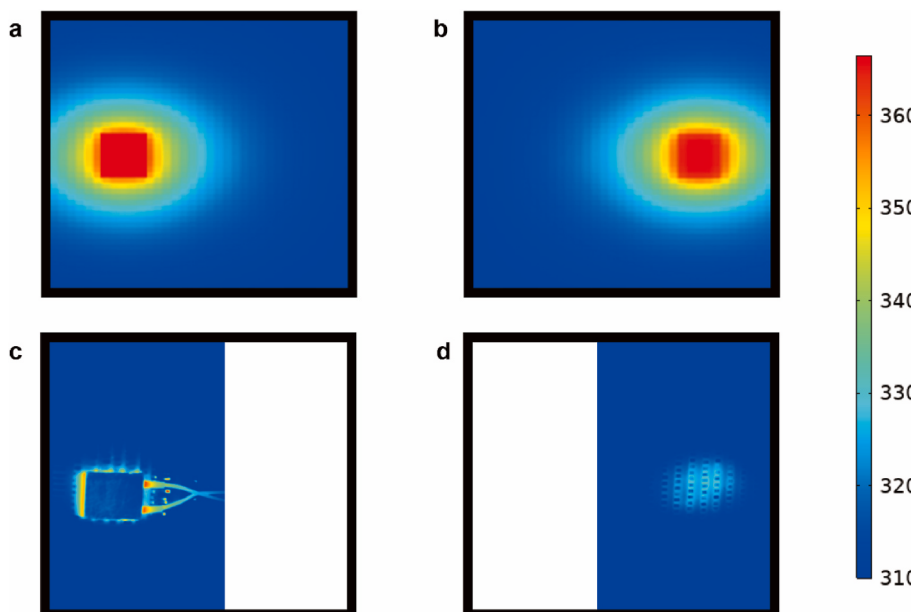


**Fig. 6.** The simulated temperature field distributions and measured temperature field distributions on the object plane and image plane of the designed thermal shifter. (a) and (b) The simulated temperature field distributions on the object plane and image plane of the designed thermal shifter, respectively. (c) and (d) The measured temperature field distributions on the object plane and image plane of the fabricated thermal shifter by IR camera, respectively. Numerical settings in a and b (e.g., settings of the materials' parameters and the temperature field distribution of each boundary and heat source in this model) are consistent with those in the experimental environment.

with previous TCDs designed by TT, the main innovations of this study include: firstly, this study achieves an out-of-plane thermal camouflages different from the in-plane thermal camouflages of previous studies. Secondly, the design method proposed in this study is a block building approach, which can be designed without coordinate transformations and other mathematical calculations. Furthermore, all TCDs with different functions designed by the proposed block building approach can be implemented with the same materials (i.e., copper-air arrays in polyurethane plates). Both simulation results and experimental measurements verify the performance of our method, which provides a new way to create out-of-plane thermal camouflages.

## Funding data

- National Natural Science Foundation of China (Nos. 61971300, 61905208, and 62175178).
- Scientific and Technological Innovation Programs (STIP) of Higher Education Institutions in Shanxi (Nos. 2019L0159 and 2019L0146).

## Declaration of competing interest

The authors declare that they have no known competing financial interests or personal relationships that could have appeared to influence the work reported in this paper.

## Data availability

Data will be made available on request.

## Appendix A. Supplementary data

Supplementary data to this article can be found online at <https://doi.org/10.1016/j.ijthermalsci.2022.107506>.

## References

- [1] J. Teyssier, S.V. Saenko, V. Dirk, M.C. Milinkovitch, Photonic crystals cause active colour change in chameleons, *Nat. Commun.* 6 (2015) 6368.
- [2] S.A. Morin, et al., Camouflage and display for soft machines, *Science* 337 (2012) 828–832.
- [3] H. Yuk, et al., Hydraulic hydrogel actuators and robots optically and sonically camouflaged in water, *Nat. Commun.* 8 (2017) 14230.
- [4] T. Kim, et al., Asymmetric optical camouflage: tuneable reflective colour accompanied by the optical Janus effect, *Light Sci. Appl.* 9 (2020) 175.
- [5] X. Du, et al., Reconfiguration, camouflage, and color-shifting for bioinspired adaptive hydrogel-based millirobots, *Adv. Funct. Mater.* 30 (2020) 1909202.
- [6] S. Zhong, W. Jiang, P. Xu, T. Liu, J. Huang, Y. Ma, A radar-infrared bi-stealth structure based on metasurfaces, *Appl. Phys. Lett.* 110 (2017), 063502.
- [7] C. Zhang, J. Yang, W. Yuan, J. Zhao, J. Dai, T. Guo, J. Liang, G. Xu, Q. Cheng, T. Cui, An ultralight and thin metasurface for radar-infrared bi-stealth applications, *J. Phys. Appl. Phys.* 50 (2017) 444002.
- [8] S. Zhong, L. Wu, T. Liu, J. Huang, W. Jiang, Y. Ma, Transparent transmission-selective radar-infrared bi-stealth structure, *Opt Express* 26 (2018) 16466–16476.
- [9] K. Wen, T. Han, H. Lu, W. Luo, L. Zhang, H. Chen, D. Liang, L. Deng, Experimental demonstration of an ultra-thin radar-infrared bi-stealth rasorber, *Opt Express* 29 (2021) 8872–8879.
- [10] T. Han, X. Bai, J. Thong, B. Li, C.W. Qiu, Full control and manipulation of heat signatures: cloaking, camouflage and thermal metamaterials, *Adv. Mater.* 26 (2014) 1731–1734.
- [11] H. Xiao, L. Wu, Illusion thermodynamics: a camouflage technique changing an object into another one with arbitrary cross section, *Appl. Phys. Lett.* 105 (2014) 1780–1782.
- [12] R. Hu, et al., Illusion Thermotics, *Adv. Mater.* 30 (2018) 1707231–1707237.
- [13] M. Pan, Y. Huang, Q. Li, H. Luo, M. Qiu, Multi-band middle-infrared-compatible camouflage with thermal management via simple photonic structures, *Nano Energy* 69 (2020) 104449.
- [14] Y. Qu, et al., Thermal camouflage based on the phase-changing material GST, *Light Sci. Appl.* 7 (2018) 26.
- [15] L. Xu, R. Wang, J. Huang, Camouflage thermotics: a cavity without disturbing heat signatures outside, *J. Appl. Phys.* 123 (2018) 245111.
- [16] T.Z. Yang, Y. Su, W. Xu, X.D. Yang, Transient thermal camouflage and heat signature control, *Appl. Phys. Lett.* 109 (2016) 121905–133111.
- [17] S. Zhou, R. Hu, X. Luo, Thermal illusion with twinborn-like heat signatures, *Int. J. Heat Mass Tran.* 127 (2018) 607–613.
- [18] Y. Li, X. Bai, T. Yang, H. Luo, C.-W. Qiu, Structured thermal surface for radiative camouflage, *Nat. Commun.* 9 (2018) 273.
- [19] G. Xu, et al., Tunable analog thermal material, *Nat. Commun.* 11 (2020) 6028.
- [20] H. Zhu, et al., Multispectral camouflage for infrared, visible, lasers and microwave with radiative cooling, *Nat. Commun.* 12 (2021) 1805.
- [21] Y. Ma, L. Lan, W. Jiang, F. Sun, S. He, A transient thermal cloak experimentally realized through a rescaled diffusion equation with anisotropic thermal diffusivity, *NPG Asia Mater.* 5 (2013) e73-e73.
- [22] D.M. Nguyen, H. Xu, Y. Zhang, B. Zhang, Active thermal cloak, *Appl. Phys. Lett.* 107 (2015), 016623.
- [23] H. Xu, X. Shi, F. Gao, H. Sun, B. Zhang, Ultrathin three-dimensional thermal cloak, *Phys. Rev. Lett.* 112 (2014), 054301.
- [24] Y. Li, et al., Temperature-dependent transformation thermotics: from switchable thermal cloaks to macroscopic thermal diodes, *Phys. Rev. Lett.* 115 (2015) 195503.
- [25] R. Hu, S. Huang, W. Meng, L. Zhou, X. Peng, Binary thermal encoding by energy shielding and harvesting units, *Phys. Rev. Appl.* 10 (2018), 054032.
- [26] H. Run, et al., Encrypted thermal printing with regionalization transformation, *Adv. Mater.* 31 (2019) 1807841–1807849.
- [27] L. Wang, B. Li, Thermal memory: a storage of phononic information, *Phys. Rev. Lett.* 101 (2008) 267203.
- [28] S. Narayana, Y. Sato, Heat flux manipulation with engineered thermal materials, *Phys. Rev. Lett.* 108 (2012) 214303.
- [29] Tiancheng, et al., Full-parameter omnidirectional thermal metadevices of anisotropic geometry, *Adv. Mater.* 30 (2018) 1804019.
- [30] T. Han, et al., Theoretical realization of an ultra-efficient thermal-energy harvesting cell made of natural materials, *Energy Environ. Sci.* 6 (2013) 3537–3541.
- [31] T. Chen, C.N. Weng, J.S. Chen, Cloak for curvilinearly anisotropic media in conduction, *Appl. Phys. Lett.* 93 (2008) 685.
- [32] A. Greenleaf, Y. Kurylev, M. Lassas, G. Uhlmann, Schrödinger's Hat: electromagnetic, acoustic and quantum amplifiers via transformation optics, *Proc. Natl. Acad. Sci. Unit. States Am.* 109 (2012) 10169–10174.
- [33] M. Raza, Y. Liu, E.H. Lee, Y. Ma, Transformation thermodynamics and heat cloaking: a review, *J. Opt.* 18 (2016), 044002.
- [34] H. Chen, C.T. Chan, P. Sheng, Transformation optics and metamaterials, *Nat. Mater.* 9 (2010) 387–396.
- [35] J. Pendry, D. Schurig, D. Smith, Controlling electromagnetic fields, *Science* 312 (2006) 1780–1782.
- [36] F. Sun, et al., Transformation optics: from classic theory and applications to its new branches, *Laser Photon. Rev.* 11 (2017) 1700034.
- [37] L. Luo, J. Luo, H. Chu, Y. Lai, Pseudo-hermitian systems constructed by transformation optics with robustly balanced loss and gain, *Adv. Photon. Res.* 2 (2021) 2000081.
- [38] M.H. Fakheri, A. Ashrafiyan, H.B. Sedeh, A. Abdolali, Experimental verification of shape-independent surface cloak enabled by nihility transformation optics, *Adv. Opt. Mater.* 9 (2021) 2100816.
- [39] H. Chu, Q. Li, B. Liu, J. Luo, S. Sun, Z. Hang, L. Zhou, L. Lai, A hybrid invisibility cloak based on integration of transparent metasurfaces and zero-index materials, *Light Sci. Appl.* 7 (2018) 50.
- [40] H.B. Sedeh, M.H. Fakheri, A. Abdolali, Advanced synthesis of meta-antenna radiation pattern enabled by transformation optics, *J. Opt.* 21 (2019), 045108.
- [41] Fei, et al., Thermal surface transformation and its applications to heat flux manipulations, *Opt Express* 27 (2019) 33757–33767.
- [42] Y. Liu, F. Sun, S. He, Fast adaptive thermal buffering by a passive open shell based on transformation thermodynamics, *Adv. Theor. Simul.* 1 (2018) 1800026.
- [43] Y. Li, et al., Thermal meta-device in analogue of zero-index photonics, *Nat. Mater.* 18 (2019) 48–54.
- [44] H.B. Sedeh, M.H. Fakheri, A. Abdolali, F. Sun, Y. Ma, Feasible thermodynamics devices enabled by thermal-null medium, *Phys. Rev. Appl.* 14 (2020) 64034.
- [45] F. Yang, B. Tian, L. Xu, J. Huang, Experimental demonstration of thermal chameleonlike rotators with transformation-invariant metamaterials, *Phys. Rev. Appl.* 14 (2020), 054024.
- [46] C.W. Nan, R. Birninger, D.R. Clarke, H. Gleiter, Effective thermal conductivity of particulate composites with interfacial thermal resistance, *J. Appl. Phys.* 81 (1997) 6692–6699.
- [47] C.E. Sten, DC fields and analytical image solutions for a radially anisotropic spherical conductor, *IEEE Trans. Dielectr. Electr. Insul.* 2 (1995) 360–367.
- [48] F. Cardarelli, Materials Handbook: A Concise Desktop Reference, Springer International Publishing, 2018.
- [49] J. Chen, et al., Synthesis, characterization and infrared emissivity study of polyurethane/TiO<sub>2</sub> nanocomposites, *Appl. Surf. Sci.* 253 (2007) 9154–9158.